

# GTFMN: GUIDED TEXTURE AND FEATURE MODULATION NETWORK FOR LOW-LIGHT IMAGE ENHANCEMENT AND SUPER-RESOLUTION

Yongsong Huang<sup>1,2</sup>, Tzu-Hsuan Peng<sup>3</sup>, Tomo Miyazaki<sup>1</sup>, Xiaofeng Liu<sup>2</sup>,  
 Chun-Ting Chou<sup>4</sup>, Ai-Chun Pang<sup>3,5</sup>, Fellow, IEEE, Shinichiro Omachi<sup>1</sup>, Senior Member, IEEE

<sup>1</sup> Graduate School of Engineering, Tohoku University, Sendai, Japan

<sup>2</sup> Dept. of Radiology & Biomedical Imaging, Yale University, New Haven, CT, USA

<sup>3</sup> Dept. of Computer Science and Information Engineering, National Taiwan University, Taipei, Taiwan

<sup>4</sup> Graduate Institute of Communication Engineering, National Taiwan University, Taipei, Taiwan

<sup>5</sup> Research Center for Information Technology Innovation, Academia Sinica, Taipei, Taiwan

## ABSTRACT

Low-light image super-resolution (LLSR) is a challenging task due to the coupled degradation of low resolution and poor illumination. To address this, we propose the Guided Texture and Feature Modulation Network (GTFMN), a novel framework that decouples the LLSR task into two sub-problems: illumination estimation and texture restoration. First, our network employs a dedicated Illumination Stream whose purpose is to predict a spatially varying illumination map that accurately captures lighting distribution. Further, this map is utilized as an explicit guide within our novel Illumination Guided Modulation Block (IGM Block) to dynamically modulate features in the Texture Stream. This mechanism achieves spatially adaptive restoration, enabling the network to intensify enhancement in poorly lit regions while preserving details in well-exposed areas. Extensive experiments demonstrate that GTFMN achieves the best performance among competing methods on the OmniNormal5 and OmniNormal15 datasets, outperforming them in both quantitative metrics and visual quality.

**Index Terms**— Super-resolution, Low-light image enhancement, Image restoration, Feature modulation, Illumination estimation

## 1. INTRODUCTION

Image super-resolution (SR) and low-light enhancement are fundamental computer vision tasks with widespread applications in areas such as autonomous driving and video surveillance[1, 2, 3]. In practical scenarios, particularly with hardware-constrained devices like vehicle dashcams, captured images often suffer from both low resolution and severe illumination degradation due to rapidly changing outdoor lighting[4, 5]. For critical situations such as accident analysis, high-quality image restoration is paramount, necessitating the simultaneous execution of super-resolution and low-light enhancement. While a two-stage approach that handles these

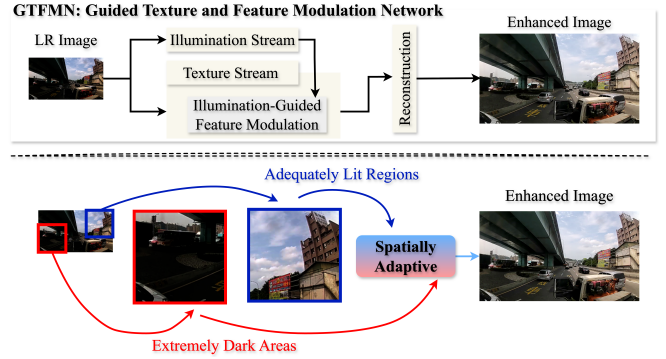


**Fig. 1.** The overall framework and core concept of GTFMN.

degradations sequentially is feasible, it inevitably introduces additional computational overhead. Therefore, developing a unified framework that addresses both issues concurrently is highly desirable.

Conventional single-stream SR networks[6, 7] often falter in this challenging domain[8, 9]. When applied directly to low-light images, they tend to amplify inherent noise and produce undesirable color shifts[10], as their feature extraction mechanisms are not designed to distinguish between signal and noise under such conditions. As illustrated in Fig.1, the core challenge is to selectively enhance extremely dark areas without over-exposing regions that are already adequately lit, demanding a spatially adaptive solution[11, 12, 13].

To address this, we propose a novel approach that explicitly decouples the problem. Instead of relying on a single network to implicitly learn both tasks, we introduce the Guided Texture and Feature Modulation Network (GTFMN, see Fig.1). Specifically, our framework is designed to first analyze the scene's illumination and subsequently leverage this analysis to guide the texture restoration process. This is realized through a novel dual-stream architecture: **1)** An Illumination Stream is designed to estimate a pixel-wise illumination map from

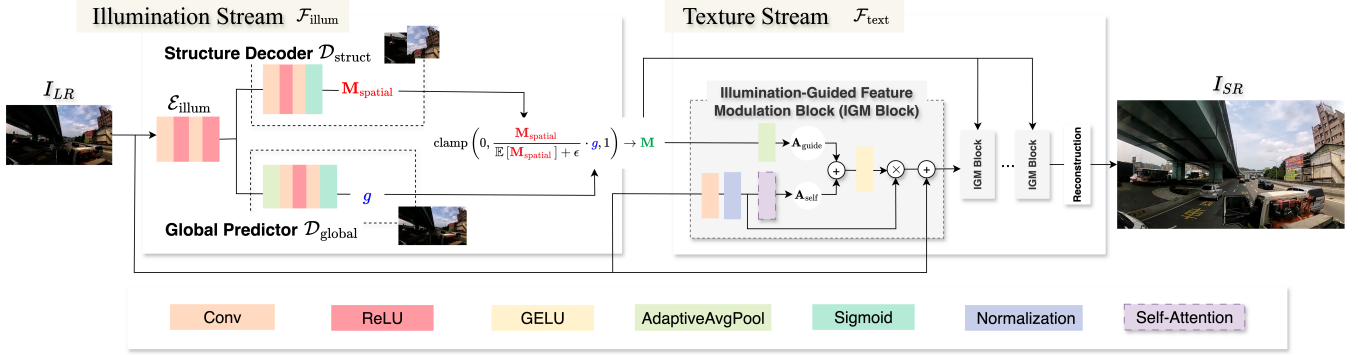


**Fig. 2.** The detailed architecture of our GTFMN. The network consists of two main branches. The **Illumination Stream** (left) takes the low-resolution input ( $I_{LR}$ ) and employs a decoupled design with a Structure Decoder and a Global Predictor to estimate a stable illumination map ( $M$ ). The **Texture Stream** (right) processes the image features through a series of Illumination-Guided Feature Modulation Blocks (IGM Blocks). Within each IGM Block, the  $M$  generates a guided attention map ( $A_{guide}$ ), which is fused with the feature-derived self-attention map ( $A_{self}$ ) to dynamically modulate the texture features. Finally, a reconstruction module produces the super-resolution image ( $I_{SR}$ ).

the low-resolution input. To enhance stability and physical plausibility, this stream further decouples the estimation of spatial light distribution and global brightness. **2)** A Texture Stream processes the image content, where a series of novel Illumination-Guided Feature Modulation Blocks (IGM Blocks) leverage the estimated illumination map to dynamically modulate texture features. This allows the network to apply enhancement adaptively across different regions.

Our contributions are as follows: First, we propose a novel dual-stream architecture that decouples the LLSR task into illumination estimation and texture restoration. Second, we introduce the IGM Block, a new module that leverages the estimated illumination as an explicit guide to achieve spatially adaptive feature modulation. Third, we validate our method through extensive experiments, which demonstrate that GTFMN achieves a favorable balance between performance and parameter count.

## 2. METHODOLOGY

Our proposed GTFMN is designed to transform a low-light, low-resolution input image  $I_{LR} \in \mathbb{R}^{H \times W \times 3}$  into a high-quality, normal-light output  $I_{SR} \in \mathbb{R}^{sH \times sW \times 3}$ , where  $H$  and  $W$  are the height and width of the input, and  $s$  is the upscaling factor. The network, denoted as  $\mathcal{G}$ , also produces an intermediate illumination map  $M \in [0, 1]^{H \times W \times 1}$ . The overall process is formulated as:

$$(I_{SR}, M) = \mathcal{G}(I_{LR}) \quad (1)$$

The architecture, depicted in Fig. 2, consists of two parallel streams followed by a feature modulation and reconstruction pipeline.

### 2.1. Illumination Stream

The Illumination Stream,  $\mathcal{F}_{\text{illum}}$ , is responsible for estimating the scene's lighting conditions. To achieve a robust estimation, we decouple this process into predicting spatial structure and global intensity. First, an encoder  $E_{\text{illum}}$  extracts features  $\mathbf{F}_{\text{enc}}$  from the input  $I_{LR}$ . Subsequently, two parallel branches operate on these features: A Structure Decoder,  $\mathcal{D}_{\text{struct}}$ , predicts the spatial illumination distribution, yielding a preliminary map  $M_{\text{spatial}} \in [0, 1]^{H \times W \times 1}$ . Further, a Global Predictor,  $\mathcal{D}_{\text{global}}$ , employs adaptive average pooling to estimate the scene's global mean brightness, producing a scalar value  $g \in [0, 1]$ .

The final illumination map  $M$  is synthesized by normalizing the spatial map and scaling it by the global intensity, ensuring its mean value aligns with the predicted global brightness. This is formally expressed as:

$$M = \text{clamp} \left( 0, \frac{M_{\text{spatial}}}{\mathbb{E}[M_{\text{spatial}}] + \epsilon} \cdot g, 1 \right) \quad (2)$$

where  $\mathbb{E}[\cdot]$  denotes the spatial mean operator and  $\epsilon$  is a small constant to prevent division by zero. This decoupled design, e.g., GTFMN, enhances the stability and physical plausibility of the estimated illumination.

### 2.2. Texture Stream and Guided Modulation

The Texture Stream is the core of the restoration process, guided by the output of the Illumination Stream. Initially, a convolution layer maps the input  $I_{LR}$  into a high-dimensional feature space, producing the initial feature map  $\mathbf{F}_0 \in \mathbb{R}^{H \times W \times C}$ .

This feature map is then processed by a series of IGM Blocks. Each block, denoted  $\mathcal{B}_i$ , refines the feature map  $\mathbf{F}_{i-1}$



**Fig. 3.** Qualitative comparison with state-of-the-art methods on the OmniNormal15 dataset for  $\times 2$  and  $\times 4$  SR.

**Table 1.** The average results of (PSNR/dB↑ MSE↓ SSIM↑ LPIPS↓) with scale factor of 2 & 4 on datasets OmniNormal5 & OmniNormal15. Best and second-best performances are marked in **bold** and underlined, respectively.

Scale	Methods	# Params. (K)	OmniNormal5				OmniNormal15			
			PSNR/dB↑	MSE↓	SSIM↑	LPIPS↓	PSNR/dB↑	MSE↓	SSIM↑	LPIPS↓
$\times 2$	SRCNN/ <i>T-PAMI 2015</i> [6]	57	34.9111	23.7764	0.9655	0.1327	34.9288	26.0693	0.9668	0.1243
	FSRCNN/ <i>ECCV 2016</i> [14]	475	36.9519	15.0543	0.9780	0.0986	37.1436	15.7841	0.9793	0.0898
	RCAN/ <i>ECCV 2018</i> [15]	12,467	25.1271	218.7846	0.9657	0.1264	24.3144	261.1591	0.9613	0.1307
	ESRGAN/ <i>ECCVW 2018</i> [16]	16,661	<u>38.1424</u>	<u>11.1514</u>	<u>0.9830</u>	<u>0.0828</u>	<u>38.1943</u>	<u>11.8353</u>	<u>0.9834</u>	<b>0.0748</b>
	SwinIR/ <i>ICCV 2021</i> [17]	11,752	37.2010	13.7718	0.9799	0.0948	37.5008	14.2757	0.9811	0.0878
	ShuffleMixer (base)/ <i>NIPS'22</i> [18]	121	37.0043	14.8764	0.9782	0.0973	37.2787	15.2924	0.9798	0.0890
	ShuffleMixer(tiny)/ <i>NIPS'22</i> [18]	108	37.4738	13.3795	0.9801	0.0928	37.6842	13.8223	0.9815	0.0842
	HAT/ <i>CVPR 2023</i> [19]	20,624	37.1974	14.0158	0.9795	0.0942	37.3550	14.8403	0.9807	0.0880
	MambaIRv2/ <i>CVPR 2025 SOTA</i> [20]	22,903	37.9634	11.6950	0.9820	0.0842	38.1523	12.2329	0.9827	0.0793
$\times 4$	<b>Ours</b>	8,784	<b>38.3420</b>	<b>10.6568</b>	<b>0.9833</b>	<b>0.0802</b>	<b>38.4256</b>	<b>11.3635</b>	<b>0.9837</b>	<u>0.0764</u>
	SRCNN/ <i>T-PAMI 2015</i> [6]	57	27.6026	119.0490	0.8523	0.2924	27.3339	141.8247	0.8478	0.2743
	FSRCNN/ <i>ECCV 2016</i> [14]	475	28.9793	87.0475	0.8912	0.2398	28.9108	100.9445	0.8912	0.2289
	RCAN/ <i>ECCV 2018</i> [15]	12,467	19.8145	692.1308	0.8109	0.3689	19.2857	790.8084	0.8082	0.3400
	ESRGAN/ <i>ECCVW 2018</i> [16]	16,661	<u>30.0527</u>	<u>66.9510</u>	<u>0.9149</u>	<u>0.2143</u>	<u>30.0691</u>	<u>78.6757</u>	<u>0.9129</u>	<u>0.2032</u>
	SwinIR/ <i>ICCV 2021</i> [17]	11,752	28.7296	92.0697	0.8850	0.2459	28.6221	106.5887	0.8855	0.2338
	ShuffleMixer (base)/ <i>NIPS'22</i> [18]	121	29.7385	72.1371	0.9079	0.2171	29.6922	85.4311	0.9065	0.2077
	ShuffleMixer(tiny)/ <i>NIPS'22</i> [18]	108	29.2293	82.0615	0.8973	0.2319	29.2774	94.1718	0.8984	0.2200
	HAT/ <i>CVPR 2023</i> [19]	20,624	28.5813	94.1024	0.8879	0.2506	28.2677	110.9638	0.8881	0.2435
	MambaIRv2/ <i>CVPR 2025 SOTA</i> [20]	22,903	29.8158	70.8697	0.9083	0.2196	29.7476	85.2837	0.9053	0.2097
	<b>Ours</b>	8,784	<b>31.1362</b>	<b>51.8216</b>	<b>0.9303</b>	<b>0.1859</b>	<b>30.5956</b>	<b>70.7727</b>	<b>0.9187</b>	<b>0.1890</b>

using the illumination map  $\mathbf{M}$  as guidance:

$$\mathbf{F}_i = \mathcal{B}_i(\mathbf{F}_{i-1}, \mathbf{M}), \quad \text{for } i = 1, \dots, N \quad (3)$$

The central mechanism within each IGM Block is the fusion of self-derived and illumination-guided attention. For an input feature  $\mathbf{F}_{in}$ , we first compute a self-attention map  $\mathbf{A}_{self}$  using a multi-scale attention layer. Next, the illumination map  $\mathbf{M}$  is passed through a small adapter network to generate a guided attention map  $\mathbf{A}_{guide}$ . These two maps are additively fused to form the final modulation signal:

$$\mathbf{A}_{final} = \mathbf{A}_{self} + \mathbf{A}_{guide} \quad (4)$$

This final attention map dynamically modulates the normalized input features through element-wise multiplication. The output of the IGM Block is produced after passing through a feed-forward network with residual connections.

Finally, the reconstruction layer  $\mathcal{F}_{recon}$ , composed of a convolution layer and a PixelShuffle operation, then upscales the deep features to generate  $I_{SR}$ .

### 3. EXPERIMENTAL RESULTS

**Datasets.** Our experiments are conducted on a custom-built dataset. The training set, named OmniTrain, comprises 1600 HR images paired with their synthetically degraded counterparts. For evaluation, we utilize two distinct test sets: OmniNormal5 and OmniNormal15, which contain 5 and 15 representative scenes, respectively. These test datasets are designed to facilitate a fair and comprehensive comparison of algorithm performance. To generate the paired data, we first analyzed a large set of real-world low-light images to establish a representative average gamma value. We then applied this gamma correction to the high-quality images to simulate low-light

**Table 2.** Ablation study on the number of blocks. The best result for each dataset is highlighted in **bold**.

# Blocks	OmniNormal5		OmniNormal15	
	PSNR (dB)	SSIM	PSNR (dB)	SSIM
16	38.0051	0.9820	38.0172	0.9821
32	37.9985	0.9820	38.2557	0.9831
64	<b>38.1061</b>	<b>0.9824</b>	<b>38.3408</b>	<b>0.9834</b>

conditions, followed by bicubic downsampling to create the final LR images. This process ensures our dataset realistically models the compound degradations encountered in practical applications.

**Metrics and Implementation Details.** We report performance using four standard metrics: Peak Signal-to-Noise Ratio (PSNR), Structural Similarity (SSIM), Mean Squared Error (MSE), and the Learned Perceptual Image Patch Similarity (LPIPS)[21] to measure perceptual quality. Our model is trained using the Adam[22] optimizer with an L1 loss function. The number of IGM Blocks is set to 64. All evaluations are conducted in the Y channel of the YCbCr color space. The learning rate is initialized at  $2 \times 10^{-4}$ . Utilizing the PyTorch framework, the model is trained with an RTX A6000 GPU.

**Quantitative Results.** As shown in Table.1, we compare GTFMN with several methods. Our model consistently outperforms all competing methods across both datasets and scaling factors ( $\times 2, \times 4$ ). Notably, for the challenging  $\times 4$  super-resolution task on OmniNormal5, GTFMN achieves a PSNR of 31.1362 dB, surpassing the second-best method, ESRGAN, by a significant margin of 1.08 dB. Furthermore, GTFMN demonstrates strong parameter efficiency, achieving these results with only 8.78M parameters, which is considerably less than large-scale models like RCAN, SwinIR, and HAT.

**Qualitative Result.** Fig. 3 provides a visual comparison of our results against other state-of-the-art methods. Visual comparisons reveal that competing models like ESRGAN and HAT tend to amplify noise and generate artifacts, particularly in the darkest regions of the image (highlighted by red boxes). In contrast, GTFMN more effectively restores textures and suppresses noise, producing results with higher fidelity. For instance, in test sample "LR 0005", our method renders the text "KPC-3316" with superior clarity and sharpness compared to all other methods. Similarly, in the "LR 0014" sample, GTFMN restores the details on the yellow sign more faithfully.

### 3.1. Ablation Study

**Effectiveness of the IGM Blocks.** We experimented with varying the number of IGM Blocks in the Texture Stream. As shown in Table 2, performance generally improves with network depth. The configuration with 64 blocks achieves the best results on both datasets, demonstrating the capacity of a

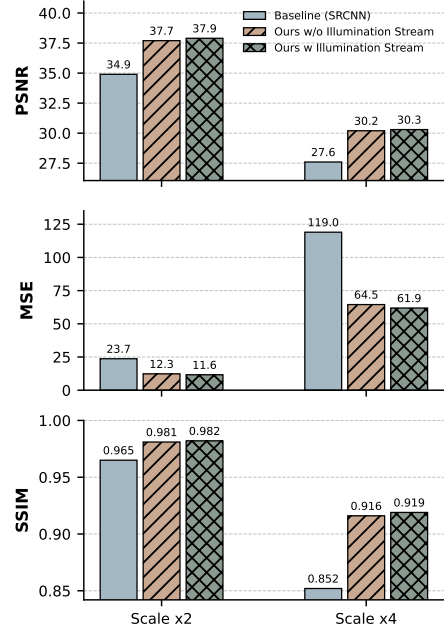


**Fig. 4.** Ablation study on the effectiveness of the Illumination Stream.

deeper network to learn more complex feature transformations. However, it is important to note that a deeper network also leads to an increase in parameter count and computational overhead. This presents a trade-off, allowing the network depth to be selected based on specific application requirements.

**Effectiveness of the Illumination Stream.** We also compare our full model against a variant where the Illumination Stream and all guidance mechanisms are removed, reducing it to a single-stream architecture. As shown in Fig.4, the full model ("Ours w Illumination Stream") largely outperforms the variant without guidance ("Ours w/o Illumination Stream") across all metrics. For instance, at scale  $\times 4$ , the inclusion of the illumination stream boosts PSNR from 30.2 dB to 30.3 dB and improves SSIM from 0.916 to 0.919. This confirms that the explicit illumination guidance is crucial for achieving high-quality restoration.

## 4. CONCLUSION

In this paper, we introduced GTFMN, a novel dual-stream network for low-light image super-resolution. By decoupling the task into illumination estimation and guided texture restoration, our model effectively addresses the coupled degradations inherent in the LLSR problem. The proposed Illumination-Guided Modulation Block enables spatially adaptive feature enhancement, leading to better performance in both quantitative metrics and visual quality. Our work provides a new and effective framework for tackling complex, multi-faceted image restoration tasks.

## 5. ACKNOWLEDGEMENT

This work was supported in part by JSPS KAKENHI Grant (JP23KJ0118, JP23K11176, and JP25K03130), the National Science and Technology Council Grant No.NSTC12-2221-E-001-028-MY3, the NVIDIA Academic Grant Program, and the Center of Data Intelligence: Technologies, Applications, and Systems, National Taiwan University (Grant No.115L900903), from the Featured Areas Research Center Program within the framework of the Higher Education Sprout Project by the Ministry of Education of Taiwan.

## 6. REFERENCES

- [1] Yongsong Huang, Zetao Jiang, Rushi Lan, Shaoqin Zhang, and Kui Pi, “Infrared image super-resolution via transfer learning and psrgan,” *IEEE Signal Processing Letters*, vol. 28, pp. 982–986, 2021.
- [2] Yongsong Huang, Tomo Miyazaki, Xiaofeng Liu, and Shinichiro Omachi, “Irsrmamba: Infrared image super-resolution via mamba-based wavelet transform feature modulation model,” *IEEE Transactions on Geoscience and Remote Sensing*, pp. 1–1, 2025.
- [3] Yongsong Huang, Tomo Miyazaki, Xiaofeng Liu, and Shinichiro Omachi, “Infrared image super-resolution: Systematic review, and future trends,” *arXiv preprint arXiv:2212.12322*, 2022.
- [4] Yan Zhuang et al., “Local sliced wasserstein feature sets for illumination invariant face recognition,” *Pattern Recognition*, vol. 162, pp. 111381, 2025.
- [5] Zunjin Zhao et al., “A non-regularization self-supervised retinex approach to low-light image enhancement with parameterized illumination estimation,” *Pattern Recognition*, vol. 146, pp. 110025, 2024.
- [6] Chao Dong et al., “Image super-resolution using deep convolutional networks,” *IEEE transactions on pattern analysis and machine intelligence*, vol. 38, no. 2, pp. 295–307, 2015.
- [7] Long Sun et al., “Spatially-adaptive feature modulation for efficient image super-resolution,” in *Proceedings of the IEEE/CVF ICCV*, 2023, pp. 13190–13199.
- [8] Kaiyang Zhou et al., “Domain generalization: A survey,” *IEEE Transactions on Pattern Analysis and Machine Intelligence*, 2022.
- [9] Lei Zhang and Xinbo Gao, “Transfer adaptation learning: A decade survey,” *IEEE Transactions on Neural Networks and Learning Systems*, 2022.
- [10] Baochen Sun et al., “Return of frustratingly easy domain adaptation,” in *AAAI*, 2016, vol. 30.
- [11] Yuanhao Cai, Hao Bian, Jing Lin, Haoqian Wang, Radu Timofte, and Yulun Zhang, “Retinexformer: One-stage retinex-based transformer for low-light image enhancement,” in *Proceedings of the IEEE/CVF international conference on computer vision*, 2023, pp. 12504–12513.
- [12] Jiesong Bai, Yuhao Yin, Qiyuan He, Yuanxian Li, and Xiaofeng Zhang, “Retinexmamba: Retinex-based mamba for low-light image enhancement,” in *International Conference on Neural Information Processing*. Springer, 2024, pp. 427–442.
- [13] Jiachen Dang, Zehao Li, Yong Zhong, and Lishun Wang, “WaveNet: Wave-Aware Image Enhancement,” in *Pacific Graphics Short Papers and Posters*, Raphaëlle Chaine, Zhigang Deng, and Min H. Kim, Eds. 2023, The Eurographics Association.
- [14] Chao Dong et al., “Accelerating the super-resolution convolutional neural network,” in *ECCV*. Springer, 2016, pp. 391–407.
- [15] Yulun Zhang et al., “Image super-resolution using very deep residual channel attention networks,” in *Proceedings of the ECCV*, 2018, pp. 286–301.
- [16] Xintao Wang et al., “Esrgan: Enhanced super-resolution generative adversarial networks,” in *Proceedings of the European conference on computer vision (ECCV) workshops*, 2018, pp. 0–0.
- [17] Jingyun Liang et al., “Swinir: Image restoration using swin transformer,” in *Proceedings of the IEEE/CVF ICCV*, 2021, pp. 1833–1844.
- [18] Long Sun et al., “Shufflemixer: An efficient convnet for image super-resolution,” *Advances in Neural Information Processing Systems*, vol. 35, pp. 17314–17326, 2022.
- [19] Xiangyu Chen et al., “Activating more pixels in image super-resolution transformer,” in *Proceedings of the IEEE/CVF CVPR*, June 2023, pp. 22367–22377.
- [20] Hang Guo, Yong Guo, Yaohua Zha, Yulun Zhang, Wenbo Li, Tao Dai, Shu-Tao Xia, and Yawei Li, “Mambairv2: Attentive state space restoration,” in *Proceedings of the Computer Vision and Pattern Recognition Conference*, 2025, pp. 28124–28133.
- [21] Jake Snell, Karl Ridgeway, Renjie Liao, Brett D Roads, Michael C Mozer, and Richard S Zemel, “Learning to generate images with perceptual similarity metrics,” in *2017 IEEE international conference on image processing (ICIP)*. IEEE, 2017, pp. 4277–4281.
- [22] Diederik P Kingma and Jimmy Ba, “Adam: A method for stochastic optimization,” *arXiv preprint arXiv:1412.6980*, 2014.